ECCOMAS Congress 2016
VII European Congress on Computational Methods in Applied Sciences and Engineering
M. Papadrakakis, V. Papadopoulos, G. Stefanou, V. Plevris (eds.)
Crete Island, Greece, 5–10 June 2016

PARAMETRIC INVESTIGATION OF THE DYNAMIC RESPONSE OF RIGID BLOCKS SUBJECTED TO SYNTHETIC NEAR-SOURCE GROUND MOTION RECORDS

Michalis Fragiadakis[1], Ioannis Psycharis[1], Yenan Cao[2] and George P. Mavroeidis[2]

[1] School of Civil Engineering,
National Technical University of Athens,
5 Iroon Polytechniou 15773, Zografou Campus, Athens, Greece
e-mail: {mfrag,ipsych}@central.ntua.gr

[2] Department of Civil and Environmental Engineering and Earth Sciences,
University of Notre Dame,
Notre Dame, IN 46556, USA
e-mail: {ycao2,g.mavroeidis}@nd.edu

Keywords: rocking block; near source; synthetic ground motion; overturning.

Abstract. *We study the seismic response of rigid block structures against synthetic pulse-like ground motion records. A large number of synthetic ground motion records are systematically produced for various magnitude-distance scenarios. More specifically, we generate pulse-like ground motions for a grid of 56 receiver stations assuming a vertical strike-slip fault. The site conditions simulate a NEHRP Class D site, while for every combination of hypocenter, magnitude and receiver location, we generate 100 realizations consisting of low- and high-frequency components. The low-frequency component is based on a four-parameter wavelet, while the specific barrier model is used for the high-frequency component. The synthetic ground motions are used to study the seismic overturning of rigid blocks of various dimensions. The low-frequency pulse is described by four-parameters which refer to the amplitude, the prevailing frequency, the phase angle and the oscillatory character of the record, on top of which the high-frequency component is added. This description allows to parametrize the seismic response and thus improve our understanding on the effect of base motion characteristics on the overturning of rigid blocks.*

1 INTRODUCTION

Following the pioneering work of Housner (1963), the problem of rocking response and overturning of free-standing blocks to earthquakes, and especially to harmonic ground motion pulses, has been the subject of intense analytical and experimental research. Despite its apparent simplicity, the problem has proven to be a difficult task due to the nonlinear behavior introduced by the impact of the block with the base and the sensitivity of the response to even trivial changes of the problem parameters. Previous studies (e.g. Muto *et al.* 1960; Yim *et al*. 1980; Ishiyama 1982; Psycharis & Jennings 1983 & 1985; Priestley *et al*. 1983; Spanos & Koh 1984; Tso & Wong 1989; Cai *et al*. 1995; Anooshehpoor *et al*. 1999; Zhang & Makris 2001; Prieto *et al*. 2004; Peña *et al*. 2007; Purvance *et al.* 2008; Kounadis 2010 & 2013; Dimitrakopoulos & DeJong 2012, among others) have revealed the complex response, including certain counterintuitive trends such as: the stability of a block subjected to a particular ground motion does not depend monotonically on the size or the slenderness of the block; overturning of a block under a certain ground motion does not necessarily imply overturning for an increase in base excitation amplitude; the amplitude of the response does not always decrease with reduction in the value of the restitution coefficient.

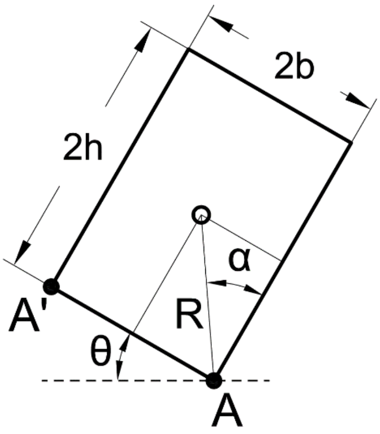

Figure 1. Rocking block geometry

In this paper, we investigate the seismic response of rigid blocks subjected to synthetic pulse-like ground motions. We consider rigid blocks of various dimensions which are subjected to pulse-like ground motions recorded at different locations with respect to the causative fault. The synthetic records consist of a low-frequency pulse, with known properties, and a high-frequency component. Following a systematic workflow, we investigate the sensitivity of the response of rigid blocks, and especially the overturning risk, to different problem parameters, such as the magnitude of the event, the distance, block dimensions and slenderness and other ground motion properties.

2 THE RIGID BLOCK PROBLEM

A rigid block of dimensions $2b\times2h$ (Figure 1) oscillates about point A (or A’), provided that the coefficient of friction is large enough to prevent sliding. The block has weight W and moment of inertia I_0 about point A (Figure 1). Assuming that the block is homogeneous and thus the center of gravity is located at height h, the block will start rocking only if the incipient ground acceleration exceeds the value of $(b/h)\cdot g$ or $g\cdot\tan(\alpha)$, where $\alpha = \mathrm{atan}(b/h)$ is the block slenderness. Note that α together with the block size parameter $R = \sqrt{h^2 + b^2}$ fully define the geometry of the block. The equation of motion of the block (Housner 1963) thus becomes:

$$I_o\ddot{\theta}(t) + mgR\sin\left[\alpha\mathrm{sgn}\theta(t) - \theta(t)\right] = -mg\ddot{u}_g(t)R\cos\left[\alpha\mathrm{sgn}\theta(t) - \theta(t)\right] \tag{1}$$

where the angle of rotation θ is the only degree of freedom. The sign function is used to define the pivot point (A or A’), which depends on the sign of θ. Therefore, when A’ is the pivot point, θ receives a negative value as implied by the sign function. For rectangular blocks, the moment of inertia becomes $I_0 = (4/3)mR^2$, while for small rotations θ, Equation (1) can be linearized:

$$\ddot{\theta}(t) = p^2\left[-\alpha\,\mathrm{sgn}\left(\theta(t)\right) + \theta(t) - \ddot{u}_g(t)/g\right] \tag{2}$$

where p denotes the characteristic frequency of the rocking block and is defined as:

$$p = \sqrt{\frac{WR}{I_0}} = \sqrt{\frac{3g}{4R}} \tag{3}$$

Dimitrakopoulos and DeJong (2012) have shown that the frequency parameter p is equal to the oscillating frequency of the block if it is viewed as a pendulum with the rocking rotation point (A or A’) being the pivot point. Damping is event-based, meaning that energy is lost only when the angle of rotation reverses and impact with the base occurs. The conservation of angular momentum just before and right after impact gives the coefficient of restitution η. This coefficient typically receives values between 0.6-0.9 and its theoretical value (Housner 1963) is:

$$\eta = \left[1 - \frac{3}{2}\sin^2\alpha\right]^2 \tag{4}$$

The equation of motion is solved numerically, while closed-form expressions for harmonic ground motions have been proposed by Dimitrakopoulos and DeJong (2012).

3 GENERATION OF BROADBAND SYNTHETIC GROUND MOTIONS

The hybrid method proposed by Mavroeidis and Papageorgiou (2003) is used to simulate broadband near-fault pulse-like ground motions. The incoherent (high-frequency) seismic radiation is synthesized using the specific barrier model (SBM) (Papageorgiou and Aki 1983). In the context of the SBM, the fault is visualized as an ensemble of non-overlapping circular subevents of equal diameter $2\rho_0$ that cover a rectangular fault with length L and width W. As the rupture front sweeps the fault plane with a rupture velocity V, a local stress drop $\Delta\sigma_L$ occurs on each subevent. The subevent rupture starts from its center and spreads radially outward with a constant spreading velocity until it is arrested by the barriers. The SBM has been calibrated to shallow crustal earthquakes of various tectonic regions (Halldorsson and Papageorgiou 2005). Given an earthquake magnitude and the tectonic region, the interdependence of other source parameters on the local stress drop $\Delta\sigma_L$ and the barrier interval $2\rho_0$ allows the causative earthquake fault to be constructed. Since the site of interest is considered to be in the “near field” of the ruptured fault, it is necessary to simulate time histories for each individual subevent of the SBM, rather than for the entire seismic event as an aggregate of subevents. The subevent time histories are subsequently summed up at the site with appropriate consideration of time delays.

On the other hand, the coherent (long-period) ground motion component is simulated using the mathematical model proposed by Mavroeidis and Papageorgiou (2003). The mathematical formulation for the representation of the near-fault velocity pulses is:

$$V(t) = 0.5A_{\mathrm{p}}\left[1+\cos\left(\frac{2\pi f_{\mathrm{p}}}{\gamma_{\mathrm{p}}}(t-t_0)\right)\right]\cos\left[2\pi f_{\mathrm{p}}(t-t_0)+\nu_{\mathrm{p}}\right], \quad t\in\left[t_0-\frac{\gamma_{\mathrm{p}}}{2f_{\mathrm{p}}}, t_0+\frac{\gamma_{\mathrm{p}}}{2f_{\mathrm{p}}}\right] \tag{5}$$

where A_{p} controls the amplitude of the signal, f_{p} is the prevailing frequency of the signal, ν is the phase of the amplitude-modulated harmonic, γ_{p} is a parameter that defines the oscillatory character of the signal, and t_0 specifies the epoch of the envelope’s peak. In addition, the pulse period T_{p} is defined as the inverse of the prevailing frequency f_{p}.

In what follows, we consider a vertical strike-slip fault in an interplate region and five scenarios with a distinct moment magnitude (M_{w} 5.5, 6.0, 6.5, 7.0, 7.5). The diameters of the subevents $2\rho_0$ are 2.9, 5.2, 9.2, 16.4 and 29.2 km for M_{w} 5.5, 6.0, 6.5, 7.0 and 7.5, respectively. According to the calibration of the SBM for interplate regimes (Halldorsson and Papageorgiou 2005), the total number of subevents that make up the SBM is typically 15. Consistent with realistic values of fault dimensions, the 15 subevents are arranged in a 5×3 pattern for events M_{w} 5.5, 6.0 and 6.5 (as illustrated in Figure 2), whereas for M_{w} 7.0 and 7.5 the subevents are placed in two rows with the upper and lower rows consisting of 8 and 7 subevents, respectively. The top edge of the fault is 0.1 km deep. The hypocenter is placed at $L/2$ along strike and $0.7W$ down dip whereas the rupture velocity is assumed to be 2.4 km/s.

The high-frequency ground motions are generated at a grid of 56 stations (Figure 2) at distances normal to the fault equal to 0.2, 1, 5, 10, 15, 20, 25 km. The spacing of the stations in the fault-parallel direction is: $-L/5$, 0, $L/5$, $2L/5$, $3L/5$, $4L/5$, $5L/5$, $6L/5$, where L is the fault length which is function of the moment magnitude M_{w}. The site characterization is assumed to be NEHRP site class D for all stations. We vary the seed number within the SBM so that 100 realizations are obtained for every combination of magnitude and receiver location. The long-period ground motion pulses are generated using the model input parameters as suggested by Mavroeidis and Papageorgiou (2003) and Halldorsson *et al.* (2011). The amplitude A_{p} is computed as A_{p} = 0.9 PGV, where the logarithm of PGV follows a normal distribution with the mean value provided by:

$$\log \mathrm{PGV} = 2.040 - 0.032 r_{\mathrm{rup}} \tag{6}$$

and a standard derivation of 0.187. The distance measure r_{rup} is defined as the closest fault-to-station distance. The pulse period T_{p} scales self-similarly with earthquake magnitude, and the logarithm of T_{p} follows a normal distribution with the mean value determined by:

$$\log T_{\mathrm{p}} = -2.9 + 0.5 M_{\mathrm{W}} \tag{7}$$

and a standard deviation of 0.143. In addition, parameter γ_{P} follows a normal distribution with a mean value of 1.93 and a standard deviation of 0.47. This distribution is left-truncated to one to ensure that all γ_{P} values are greater than one. Finally, the phase angle follows a normal distribution with mean 1.83 and standard deviation of 0.98. Note that for every combination of magnitude and receiver location, 100 samples for each model parameter (e.g. A_{p}, f_{p}, v_{p} and γ_{P}) are generated using Monte Carlo sampling. Finally, the long-period components of ground motion are superimposed on the high-frequency ground motions, with the initiation of the pulses aligned with time incident corresponding to 1% of the Arias intensity of the high-frequency motions.

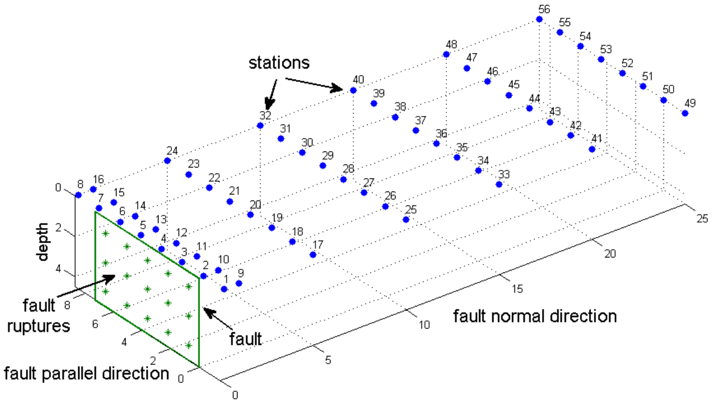

Figure 2 Fault geometry and grid of receivers (stations).

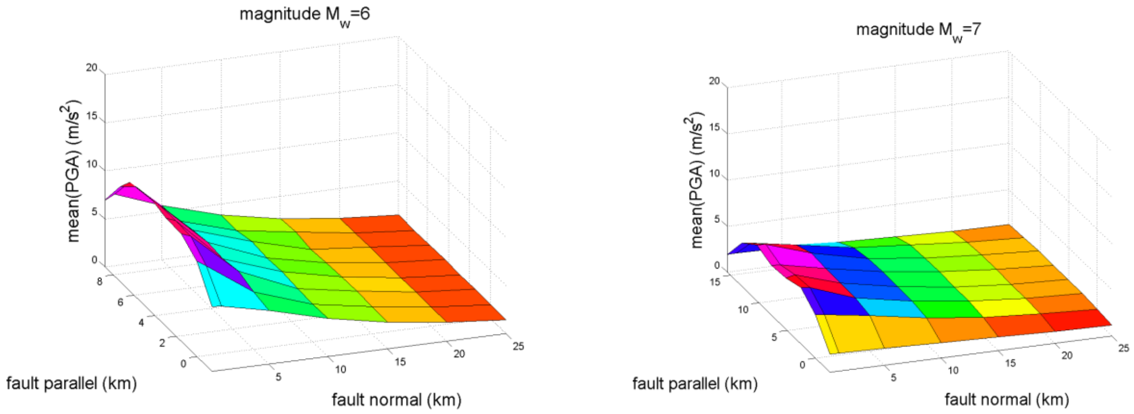

(a) (b)

Figure 3 Mean *PGA* values of the synthetic ground motion records for: (a) M_{w} = 6.0, (b) M_{w} = 7.0. Smaller M_{w} events produce larger PGA values.

Figure 3 shows the spatial distribution of the mean peak ground acceleration (*PGA*) of the synthetic broadband near-fault ground motions. For both M_{W} cases shown, larger mean *PGA* values are produced in the center of the fault-parallel direction that is closer to the epicenter, while the mean *PGA* attenuates as the distance in the fault-normal direction increases. Furthermore, the mean *PGA* values are larger for events of smaller magnitude (Figure 3). This was first observed empirically by Somerville (2000), while Mavroeidis and Papageorgiou (2003) and Mavroeidis *et al.* (2004) discussed and explained mathematically that acceleration pulses generated by smaller earthquakes are typically stronger i.e., they have higher amplitude but shorter duration than acceleration pulses of larger earthquakes. However, once the high-frequency component is added to the pulse-type motions, this trend may be reversed.

4 PRELIMINARY RESULTS

4.1 Magnitude-distance plots

We consider twelve rigid block configurations with aspect ratio $\lambda = h/b$ equal to 2, 3, 5, 10 and characteristic frequencies p = 1.5, 2.5, 5.0. The grid consists of 56 receiver stations and, for every station and block configuration, we perform block response history analysis using 100 forward-directivity synthetic ground motions. Thus for every station, we perform 12000 rigid block response history analyses. Unless otherwise specified, all analyses refer to a fixed value of the coefficient of restitution η = 0.9.

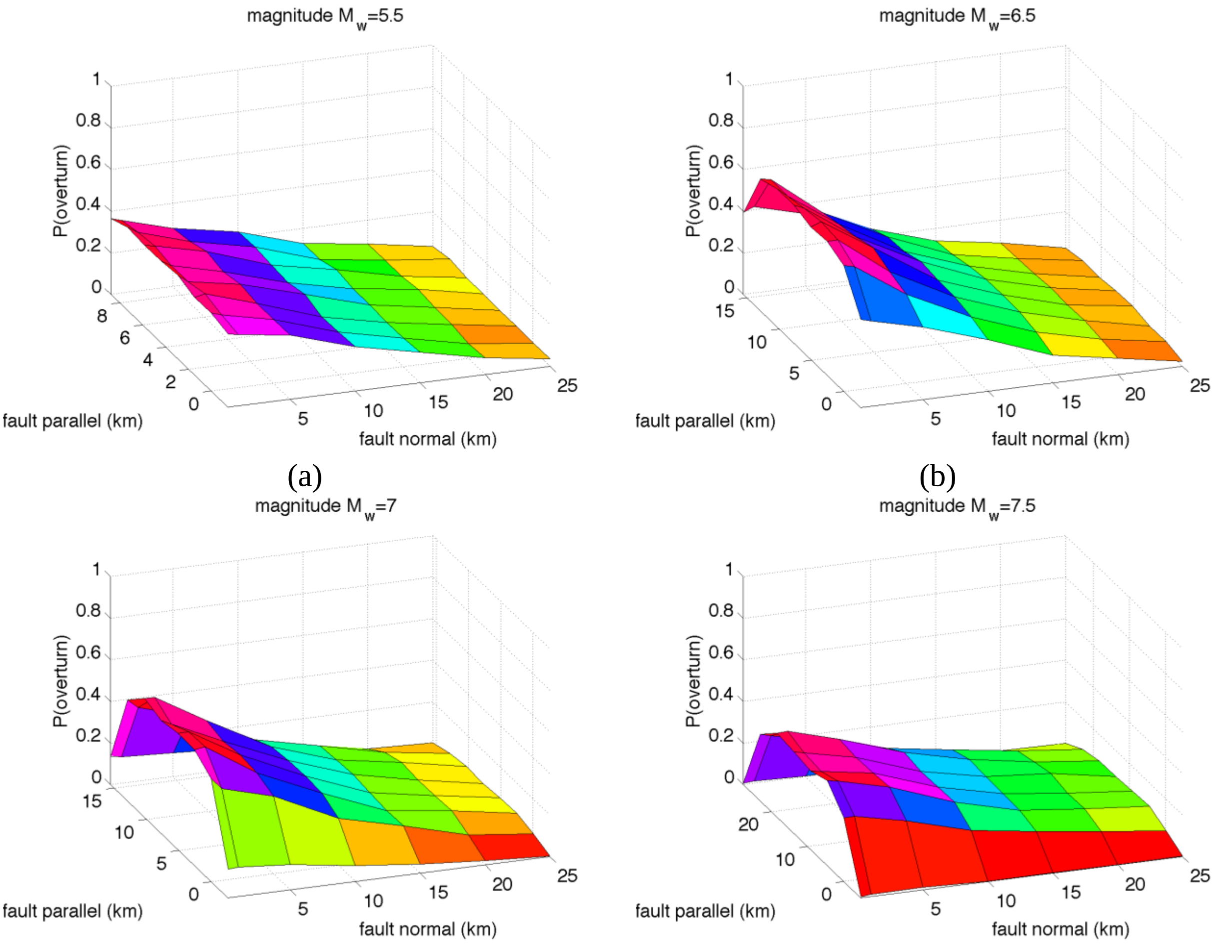

(a) (b)

(c) (d)

Figure 4 Probability of block overturning: (a) M_w = 5.5, (b) M_w = 6.5, (c) M_w = 7.0, (d) M_w = 7.5.

Figure 4 presents contour plots of the probability of block overturning. Four M_w scenarios, M_w = 5.5, 6.5, 7.0 and 7.5 are shown. The highest probabilities are observed for the M_w = 6.5 case, while smaller probabilities were obtained for the M_w = 5.5 and M_w = 7.5 ground motions. Compared to the PGA plots of Figure 3, the spatial distribution is the same, but the overturning probabilities decrease for large magnitudes. This is due to the fact that large magnitude events produce weaker and longer pulses although they have a longer duration and a stronger high-frequency component.

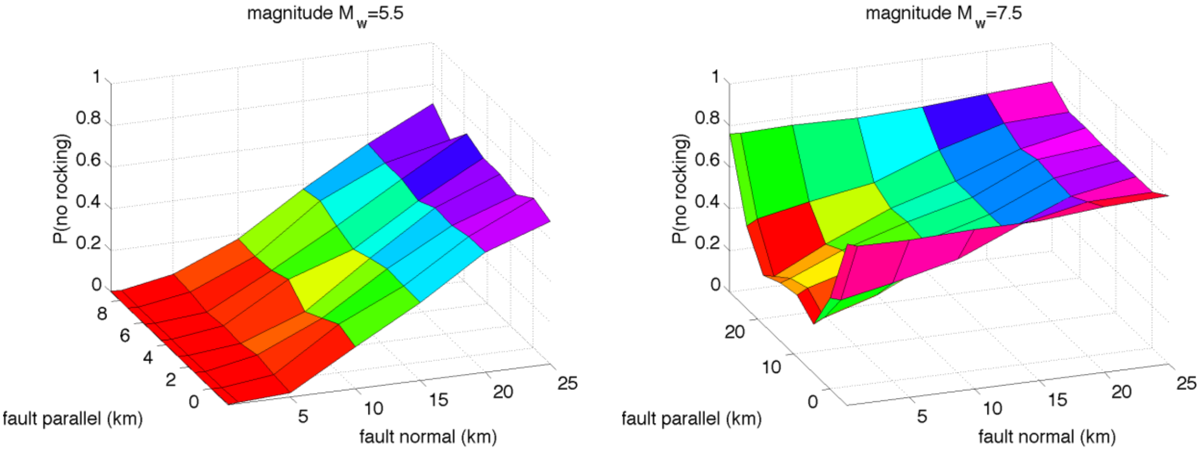

(a) (b)

Figure 5 Probability of not initiating rocking for the grid of stations: (a) M_w = 5.5, (c) M_w = 7.5.

Figure 5 shows the empirical probability that the ground motion is not strong enough to initiate rocking. It is reminded that a block starts rocking only if the *PGA* of the incipient ground motion exceeds $g \cdot \tan(\alpha)$. For the M_w = 5.5 case, practically all ground motions trigger rocking for small distances from the fault, while for stations far from the fault the probability that rocking is not initiated becomes very high. On the other hand, for the M_w = 7.5 case, the probability that no rocking is initiated is quite high even at sites very close to the fault (Figure 5b).

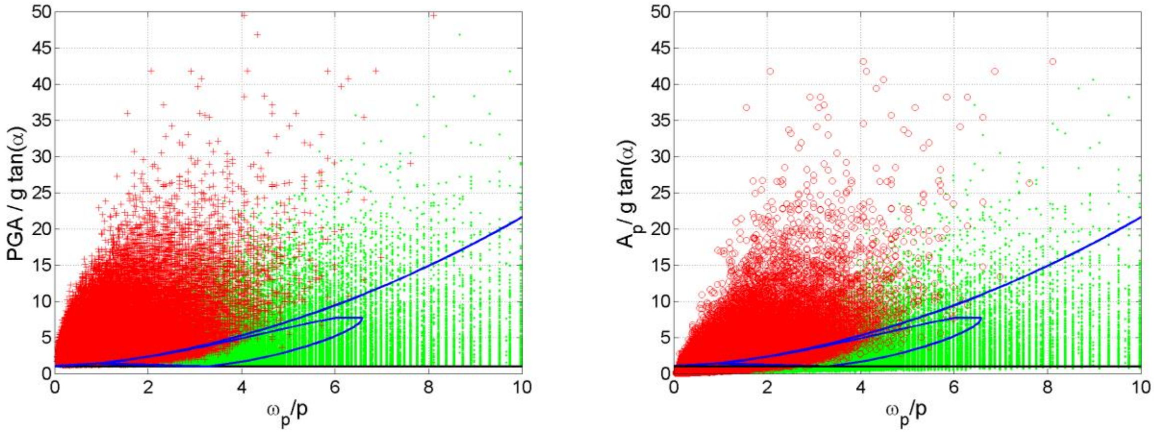

(a) (b)

Figure 6 PGA vs Ap. The blue lines refer to the closed-form expression of stable-unstable threshold for sine excitation according to Dimitrakopoulos and DeJong (2012).

4.2 Overturning spectra

The results are grouped in Figure 6 in stable-unstable plots in the acceleration-frequency domain. In Figure 6a, the normalized *PGA* with respect to the critical acceleration for the initiation of rocking, $g \cdot \tan\alpha$, is plotted versus the normalized pulse period, ω_p/p, while in Figure 6b the normalized pulse acceleration, A_p, is plotted versus ω_p/p. Red points correspond to blocks that overturned and green points to blocks that did not overturn. Blocks that were not set to rocking motion are not shown; thus, $PGA/(g \cdot \tan\alpha)$ is larger than one for all points shown in Figure 6a. However, $A_p/(g \cdot \tan\alpha)$ can be smaller than one, as shown in Figure 6b.

These plots are referred as "overturning spectra", since the horizontal axis of Figure 6 measures frequency, while the vertical axis measures the intensity of the ground motion. Angle α controls the slenderness of the block (Figure 1), while parameter p accounts for the size of the block.

The two plots of Figure 6, which look similar, define the region in which the block might overturn. In both plots we also show, for comparison, with solid blue lines the closed-form solution of Dimitrakopoulos and DeJong (2012) that define the safe-unsafe threshold for a full sine pulse with amplitude equal to the PGA or the pulse amplitude A_p of our synthetic records and frequency ω_p equal to that of the low-frequency pulse. The sinusoidal ground motions are assumed symmetric (i.e. $v = 0$). The following observations can be made looking at Figure 6:

- $PGA/(g \cdot \tan\alpha)$ is preferable over $A_p/(g \cdot \tan\alpha)$, since it is easier to calculate and respects the condition that rocking will immense only if $PGA/(g \cdot \tan\alpha) \geq 1$.
- The use of a sinusoidal pulse is overall more conservative.
- As we move to the right side of each plot of Figure 6, the points shown refer to blocks that are either large (large R and small p) or are subjected to high frequency ground motions (large ω_p values). Therefore, these results show that overturning is rather improbable to occur in such cases. This seems to be true for ω_p/p larger than 8, independently of the amplitude of the normalized acceleration.
- On the left edge of the plots, specifically for values of ω_p/p smaller than about 2, corresponding to ground motions containing long-period pulses (small ω_p values) or to small-size blocks (large p values), overturning occurs for all ground motions capable to initiate rocking.
- The apparent limit between the safe and the unsafe region implies only that the blocks on the safe side do not overturn. In other words, there are many blocks on the "unsafe" region that did not overturn. In this sense, the threshold between the safe-unsafe regions corresponds to the minimum normalized ground acceleration $PGA/(g \cdot \tan\alpha)$ for each value of ω_p/p that could topple the block, without meaning that all excitations with larger values of $PGA/(g \cdot \tan\alpha)$ will cause overturning.
- Compared to our results, the sinusoidal ground motions are more conservative for ω_p/p values that exceed 6. Beyond this limit, our broadband simulations yield that the blocks do not overturn, as opposed to the case of sinusoidal pulse where the blocks are safe or their response does not depend on the $PGA/g \cdot \tan(\alpha)$ parameter.

5 SENSITIVITY ANALYSIS

5.1 Effect of distance and magnitude

In Figure 7, the probability of block overturning versus the magnitude of the event is shown for several distances. The black solid line denotes the average trend. It is evident that the probability of block overturning is affected by both magnitude and distance. Concerning the effect of distance, small distances result to higher probabilities of block overturning, as expected. However, concerning the effect of magnitude, it is seen that the overturning probability does not monotonically increase with magnitude as one would expect, since, for events of magnitude larger than $M_w = 6.5$, the overturning probability reduces as the magnitude increases. This counter-intuitive response is attributed to the saturation of the *PGV* for earthquakes with magnitude larger than 6.5 while the period of the pulse is increasing exponentially with the magnitude (Eq. (7)). As a result, the directivity pulse has small acceleration amplitude for large magnitudes, which is not capable to produce intense rocking.

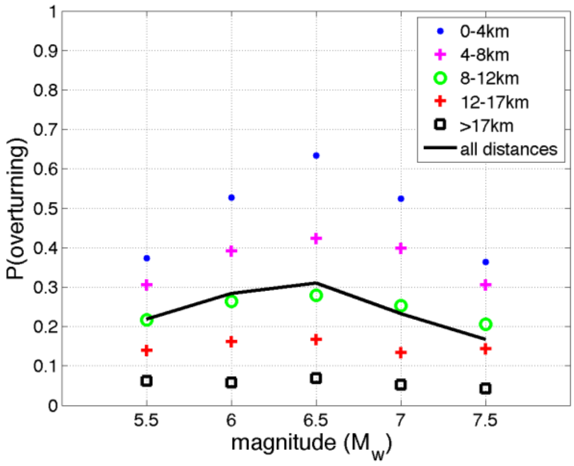

Figure 7 Variation of the probability of block overturning with magnitude and rupture distance. The black solid line denotes the average trend.

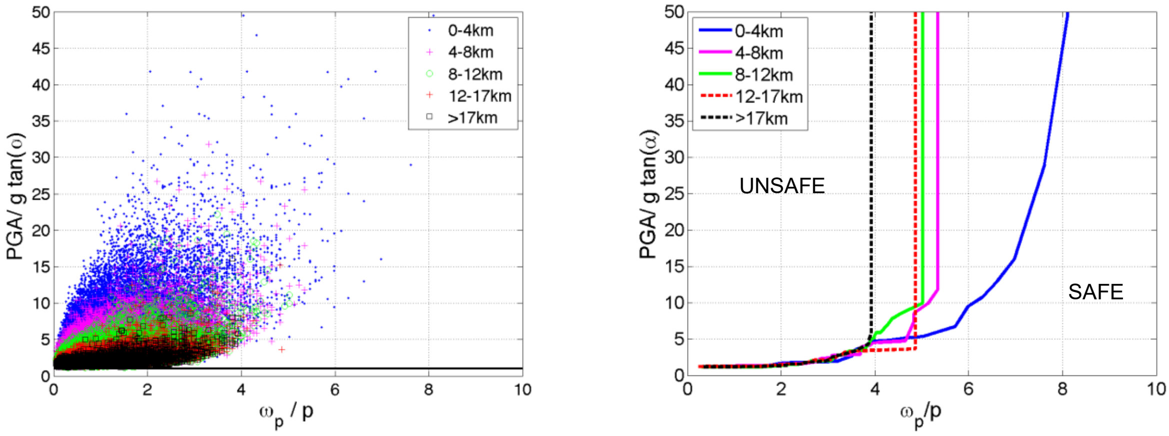

(a) (b)

Figure 8 Clustering of the ground motions that caused block overturning with respect to the rupture distance: (a) all simulations; (b) envelope curves indicating the threshold between safe and unsafe regions.

Further insight on the dependence of the block overturning probability with distance and magnitude is offered by Figure 8 and Figure 9, respectively. Figure 8 shows the effect of distance on the block overturning spectra. The left plot (Figure 8a) clusters the data depending on the distance, while Figure 8b shows the threshold curves that define the safe and the unsafe regions, allowing a better comparison. The number of blocks that overturn decrease with distance as also indicated by the overturning probabilities of Figure 7, which is attributed to the fact that the *PGA*s decrease at large-distances (Figure 3). However, as evident from Fig. 8b, the distance does not affect the safe-unsafe threshold for small values of ω_p/p, but only for blocks with $\omega_p/p \geq 4$, for which the unsafe region expands to the right for small-distant events.

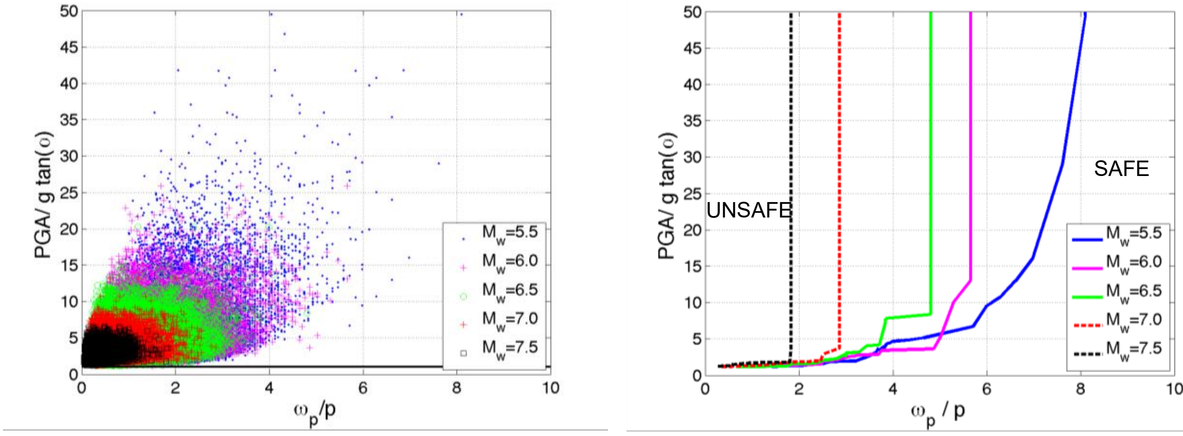

(a) (b)

Figure 9 Clustering of the ground motions that caused block overturning with respect to moment magnitude Mw: (a) all simulations; (b) envelope curves indicating the threshold between safe and unsafe regions.

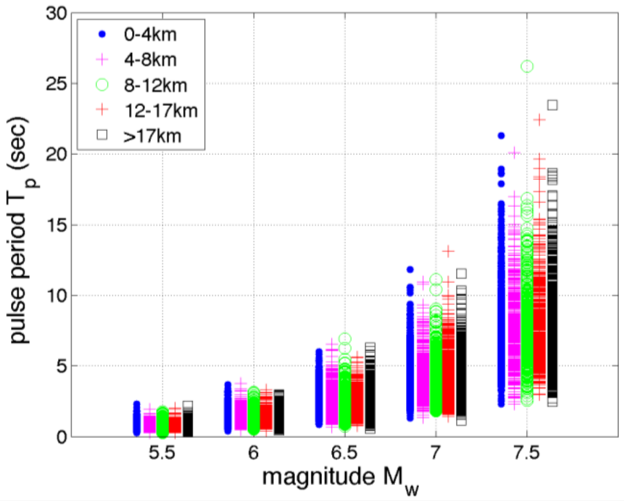

Figure 10 Relationship of the period T_p of the directivity pulse with moment magnitude M_w and distance. As M_w increases longer period values are obtained, while there is no dependence with respect to the distance.

Figure 9 shows the effect of moment magnitude M_w on the block overturning. The effect of M_w is strong, since the different magnitudes have distinct threshold curves (Figure 9b). This is due to the fact that both *PGA* and ω_p depend on the magnitude. As shown in Figure 3, events of small M_w (e.g. M_w=5.5) produce larger PGA values than larger magnitudes (e.g. M_w=6.5), although the failure probabilities do not follow this trend (Figure 7). On the other hand, ω_p decreases quickly with amplitude due to the exponential increase of the pulse period T_p (Figure 10), which means that only small values of ω_p/p can be attained for large-magnitude events. In this sense, for a given block (given p), the normalized frequency ω_p/p decreases abruptly as M_w increases and, therefore, the safe-unsafe threshold moves to the left for the range of the block dimensions examined (block size is measured by parameter p).

Another interesting conclusion that can be drawn from Figure 9b is that, for values of $\omega_p/p < 3$ the minimum PGA required to overturn a block is almost equal or slightly larger to the one needed to set it on rocking motion, since $PGA/(g{\cdot}\tan\alpha)$ is close to unity. For events with large magnitude M_w (larger than 7.0), this means that, if the ground excitation is strong enough to trigger rocking, it will most probably cause overturning too. However, for events of smaller M_w, for which values of $\omega_p/p > 3$ can be attained, the minimum PGA required to overturn a block is significantly larger than the one needed to initiate rocking (equal to $g{\cdot}\tan\alpha$).

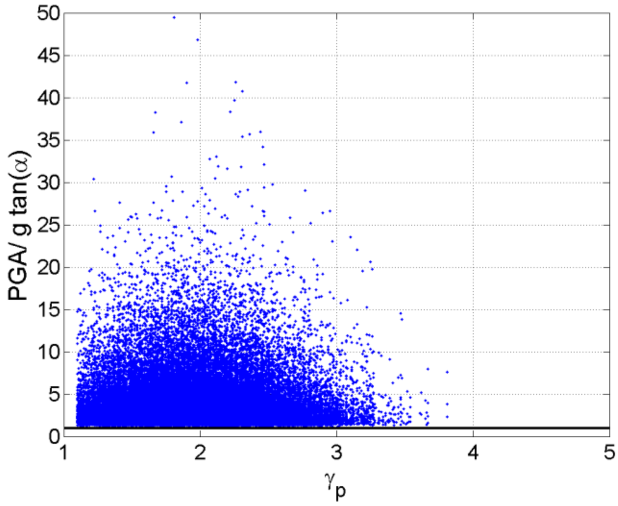

Figure 11 Distribution of the normalized PGA of the ground motions that caused overturning with the γp parameter that controls the oscillatory character of the ground motion.

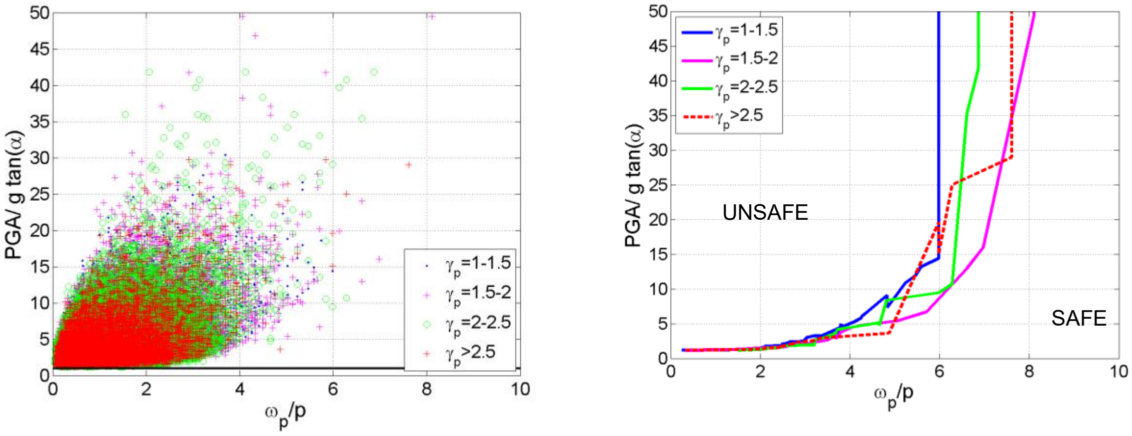

(a) (b)

Figure 12 Clustering of the data with respect to γ_p: (a) all simulations that cause block overturning, (b) envelope curves indicating the threshold between safe and unsafe regions.

5.2 Effect of the oscillatory character of the directivity pulse (γ_P parameter)

The γ_P parameter is a constant of the wavelet proposed by Mavroeides and Papageorgiou (2003) that defines the oscillatory character (i.e. zero crossings) of the signal. This parameter was assumed normally distributed when the synthetic records were generated. Figure 11 shows the analyses that overturned the blocks as function of γ_P versus the normalized $PGA/(g\cdot\tan\alpha)$ intensity. The distribution of the analyses with respect to the values of γ_P resembles that of a normal distribution. Furthermore, Figure 12 shows the overturning spectra when the results are clustered with respect to γ_P. Both the cloud plots of Figure 12a and the threshold lines of Figure 12b indicate that γ_P has a small effect on the overturning of the blocks.

5.3 Effect of block properties

5.3.1. Sensitivity to the coefficient of restitution η

The coefficient of restitution η controls the damping of the rocking motion. Figure 13b shows the threshold curves of the overturning spectra (e.g. Figure 6a) for different values of the coefficient of restitution η, namely η = 0.7, 0.8 and 0.9. Practically there is no difference between η = 0.8 and 0.9, while η = 0.7 shifts the threshold curves slightly to smaller ω_P/p values. Therefore, the effect of η, in general, is small, although there are cases where this parameter may alter the results. This conclusion is compatible with the results of past studies based on pulse-like ground motions, as the ones shown in Figure 13b obtained with the aid of the closed-form relationships of Dimitrakopoulos and DeJong (2012). In this case, the coefficient of restitution affects only the closed-loop curves, which refer to block overturning after one impact, while the monotonically increasing upper curve, which corresponds to the threshold of overturning without impact, is independent of the coefficient of restitution.

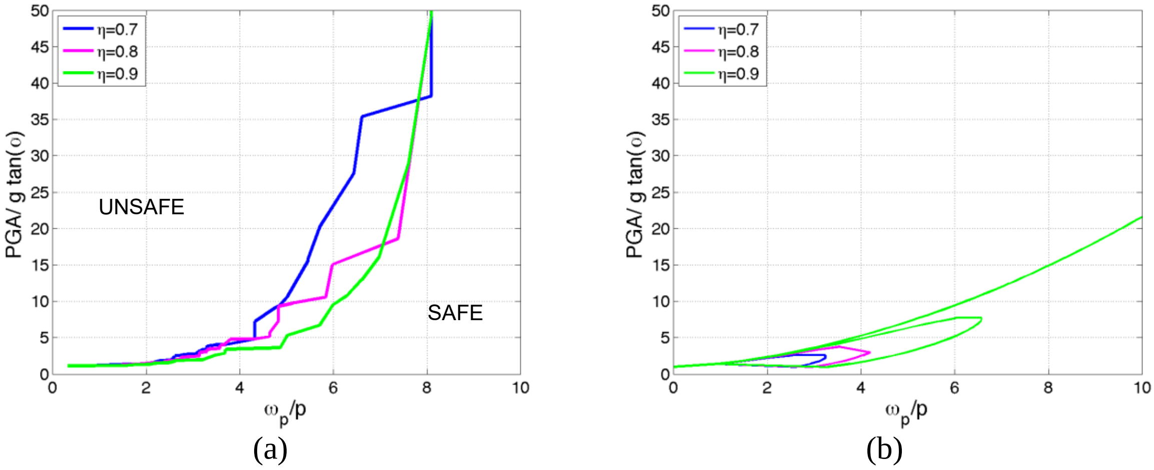

(a) (b)

Figure 13 Effect of the coefficient of restitution η on overturning spectra: (a) this study; (b) obtained using sinusoidal pulses (Dimitrakopoulos & DeJong 2012).

5.3.2. Effect of block slenderness

Figure 14 shows the effect of the block slenderness ratio $\lambda = h/b$, i.e. the aspect ratio of the block. The h/b values considered are: 2, 3, 5 and 10, corresponding to slenderness angles α equal to 26.5, 18.4, 11.3 and 5.7 degrees, respectively. As expected, slender blocks are more likely to overturn, as shown in Figure 14a, since they set to rocking motion for records with small enough *PGA*. Furthermore, slender blocks topple for significantly smaller angle of rotation than stocky ones, therefore, they are more vulnerable to small-period ground motions. This is the reason that the threshold curves of the overturning spectra move towards larger ω_p/p values as λ increases (Figure 14b).

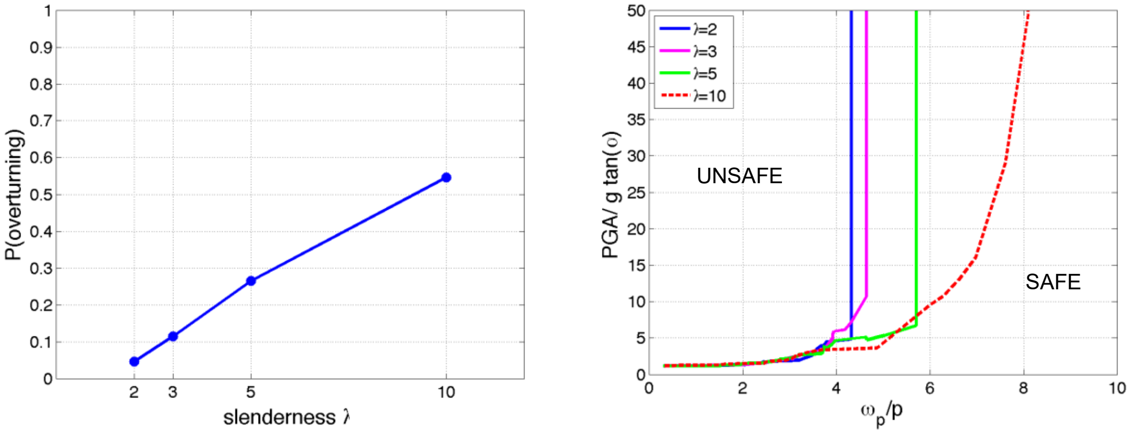

(a) (b)

Figure 14 Overturning spectra for different values of the slenderness ratio λ of the blocks: (a) overturning probability versus λ; (b) overturning spectra.

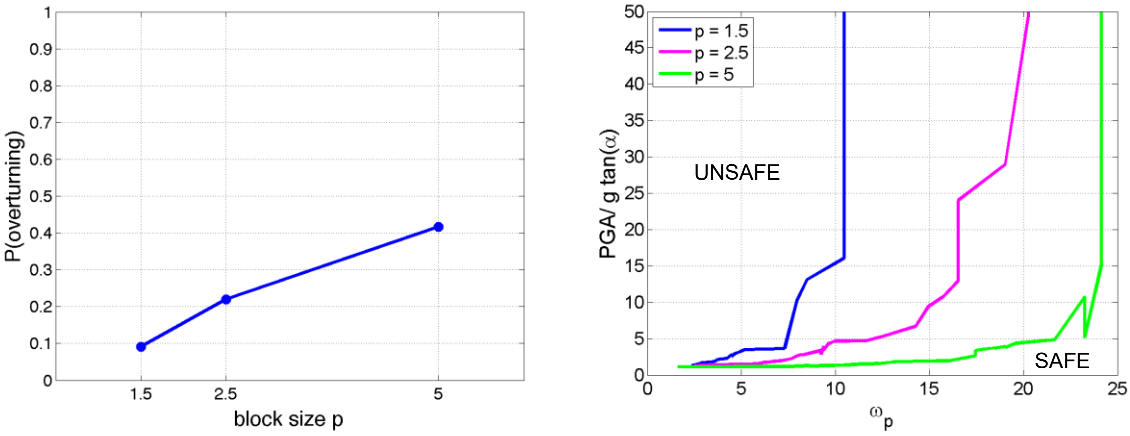

(a) (b)

Figure 15 Effect of the frequency parameter p on the response of the block: (a) overturning probability versus p; (b) overturning spectra (note that the horizontal axis is not divided with p).

5.3.3. Effect of block size

In Figure 15, we examine the effect of the frequency parameter p which is used to measure the size of the block according to Eq. (3). We examine blocks with p = 1.5, 2.5 and 5, which correspond to blocks with half diameter R = 3.3 m, 1.18 m and 0.30 m, respectively. Figure 15a shows the scale effect on the probability of overturning, which was first observed by Housner (1963), with smaller blocks (larger p) been more vulnerable than larger ones (smaller p) of the same aspect ratio. This is also shown in Figure 15b, in which the safe-unsafe thresholds of the overturning spectra are shown w.r.t. the pulse frequency ω_p. It is evident that small blocks overturn even for high-frequency ground motions, for which large blocks of the same aspect ratio are safe.

6 CONCLUSIONS

There are several parameters that control the seismic response of rigid block structures when subjected to pulse-like ground motion records. This paper offers a systematic investigation on the impact of several critical parameters through generating a large number of synthetic ground motion records and considering receiver locations at different places with respect to the fault. The response is post-processed in the form of overturning spectra, i.e. plots of the peak ground acceleration normalized by the critical acceleration required to trigger rocking ($PGA/g{\cdot}\tan\alpha$) versus the pulse frequency normalized by the characteristic frequency of the block (ω_p/p), from which the effect of various parameters on the threshold between the safe (no overturning) and unsafe (overturning) regions is investigated. The results show that the moment magnitude M_w is important, as it affects the pulse period T_p, while the effect of the distance is of lesser importance. Concerning the parameters of the directivity pulse, the oscillatory character of it (γ_p parameter) and the position of the hypocenter along the fault do not affect the results significantly. The same holds for the coefficient of restitution η, in contrast to the slenderness and the size of the block, which play an important role to the probability of overturning.

REFERENCES

[1] Anooshehpoor A, Heaton TH, Shi B & Brune JN. Estimates of the ground accelerations at Point Reyes station during the 1906 San Francisco earthquake. *Bulletin of the Seismological Society of America*, **89**(4), 845-853, 1999.

[2] Atkinson GW & Silva W. Stochastic modeling of California ground motions. *Bulletin of Seismological Society of America*, **90**, 255-274, 2000.

[3] Cai GQ, Yu JS & Lin YK. Toppling of rigid block under evolutionary random base excitations. *Journal of Engineering Mechanics - ASCE*, **121**(8), 924-929, 1995.

[4] DeJong MJ & Dimitrakopoulos EG. Dynamically equivalent rocking structures. *Earthquake Engineering and Structural Dynamics*, **43**(10), 1543-1563, 2014.

[5] Dimitrakopoulos EG & DeJong MJ. Revisiting the rocking block: Closed-form solutions and similarity laws. *Proceedings of the Royal Society A: Mathematical, Physical and Engineering Sciences*, **468** (2144), 2294-2318, 2012.

[6] Dimitrakopoulos EG & Paraskeva TS. Dimensionless fragility curves for rocking response to near-fault excitations. *Earthquake Engineering and Structural Dynamics*, **44**(12), 2015-2033, 2015.

[7] Halldorsson B & Papageorgiou AS (2005). Calibration of the specific barrier model to earthquakes of different tectonic regions, *Bulletin of the Seismological Society of America* **95**, 1276–1300.

[8] Halldorsson B, Mavroeidis GP & Papageorgiou AS (2011). Near-fault and far-field strong ground-motion simulation for earthquake engineering applications using the specific barrier model, *Journal of Structural Engineering-ASCE* **137**, 433-444.

[9] Housner GW. The behavior of inverted pendulum structures during earthquakes. *Bulletin of Seismological Society of America*, **53**, 403-417, 1963.

[10] Ishiyama Y. Motion of rigid bodies and criteria for overturning by earthquake excitations. *Earthquake Engineering and Structural Dynamics,* **10**, 635-650, 1982.

[11] Kounadis AN. On the dynamic overturning instability of a rectangular rigid block under ground excitation. *Open Mechanics Journal*, **4**, 43-57, 2010.

[12] Kounadis AN. Parametric study in rocking instability of a rigid block under harmonic ground pulse: A unified approach. *Soil Dynamics and Earthquake Engineering,* **45**, 125-143, 2013.

[13] Mavroeidis GP & Papageorgiou AS. A mathematical representation of near-fault ground motions. *Bulletin of Seismological Society of America*, **93**, 1099-1131, 2003.

[14] Mavroeidis, GP, Dong G. & Papageorgiou AS Near-fault ground motions, and the response of elastic and inelastic single-degree-of-freedom (SDOF) systems, *Earthquake Engineering and Structural Dynamics*, **33** (9), 1023-1049, 2004.

[15] Muto K, Umemura H & Sonobe Y. Study of overturning vibration of slender structures. *Proc. 2nd World Conference on Earthquake Engineering*, Tokyo, Japan, 1960.

[16] Papageorgiou AS & Aki K (1983). A specific barrier model for the quantitative description of inhomogeneous faulting and the prediction of strong ground motion. I. Description of the model, *Bulletin of the Seismological Society of America* **73**, 693-722.

[17] Peña F, Prieto F, Lourenço PB, Campos Costa A & Lemos JV. On the dynamics of rocking motion of single rigid-block structures. *Earthquake Engineering and Structural Dynamics,* **36**, 2383-2399, 2007.

[18] Priestley MJN, Evision RJ & Carr AJ. Seismic response of structures free to rock on their foundations. *Bulletin of the New Zealand National Society of Earthquake Engineering*, **11**, 141-150, 1983.

[19] Prieto F, Lourenço PB & Oliveira CS. Impulsive Dirac-delta forces in the rocking motion. *Earthquake Engineering and Structural Dynamics,* **33**(7), 839-857, 2004.

[20] Psycharis IN & Jennings PC. Rocking of slender bodies allowed to uplift. *Earthquake Engineering and Structural Dynamics,* **11**, 57-76, 1983.

[21] Psycharis IN & Jennings PC. Upthrow of objects due to horizontal impulse excitation. *Bulletin of the Seismological Society of America*, **75(**2), 543-561, 1985.

[22] Purvance MD, Anooshehpoor A & Brune JN. Freestanding block overturning fragilities: Numerical simulation and experimental validation. *Earthquake Engineering and Structural Dynamics*, **37**, 791-808, 2008.

[23] Somerville P. New developments in seismic hazard estimation, in Proc. of the Sixth Int. Conf. on Seismic Zonation, Palm Springs, California, 12–15 November 2000.

[24] Spanos PD & Koh AS. Rocking of rigid bodies due to harmonic shaking. *Journal of Engineering Mechanics - ASCE,* **110**(11), 1627-1642, 1984.

[25] Tso WK & Wong CM. Steady state rocking response of rigid block. Part I: Analysis. *Earthquake Engineering and Structural Dynamics*, **18**, 89-106, 1989.

[26] Yim CS, Chopra AK & Penzien J. Rocking response of rigid bodies to earthquakes. *Earthquake Engineering and Structural Dynamics*, **8**, 565-587, 1980.

[27] Zhang J & Makris N. Rocking response of free-standing blocks under cycloidal pulses. *Journal of Engineering Mechanics - ASCE*, **127**, 473-483, 2001.